THE JOURNAL OF PHYSICAL CHEMISTRY Letters

Letter

Cite This: J. Phys. Chem. Lett. 2019, 10, 6293−6300

pubs.acs.org/JPCL

Multistate Multiconfiguration Quantum Chemical Computation of the Two-Photon Absorption Spectra of Bovine Rhodopsin

Samira Gholami,[†] Laura Pedraza-González,[‡] Xuchun Yang,[†] Alexander A. Granovsky,[§] Ilya N. Ioffe,*[,∥] and Massimo Olivucci*[,†,‡]

[†]Department of Chemistry, Bowling Green State University, Bowling Green, Ohio 43403, United States

[‡]Department of Biotechnology, Chemistry and Pharmacy, Università di Siena, via A. Moro 2, I-53100 Siena, Siena, Italy

[§]Firefly Project, Moscow 117593, Russia

[∥]Department of Chemistry, Lomonosov Moscow State University, 119991 Moscow, Russia

Supporting Information

ABSTRACT: Recently, progress in IR sources has led to the discovery that humans can detect infrared (IR) light. This is hypothesized to be due to the two-photon absorption (TPA) events promoting the retina dim-light rod photoreceptor rhodopsin to the same excited state populated via one-photon absorption (OPA). Here, we combine quantum mechanics/molecular mechanics and extended multiconfiguration quasi-degenerate perturbation theory calculations to simulate the TPA spectrum of bovine rhodopsin (Rh) as a model for the human photoreceptor. The results show that the TPA spectrum of Rh has an intense $S_0 \rightarrow S_1$ band but shows also $S_0 \rightarrow S_2$ and $S_0 \rightarrow S_3$ transitions whose intensities, relative to the $S_0 \rightarrow S_1$ band, are significantly increased when compared to the corresponding bands of the OPA spectrum. In conclusion, we show that IR light in the 950 nm region can be perceived by rod photoreceptors, thus supporting the two-photon origin of the IR perception. We also found that the same photoreceptor can perceive red (i.e., close to 680 nm) light provided that TPA induces population of S_2.

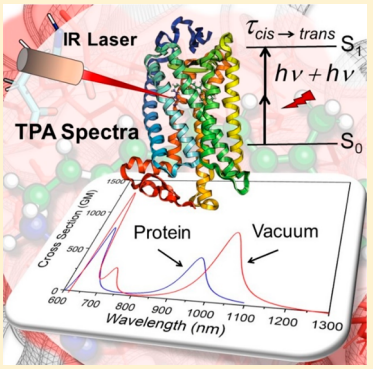

The vertebrate dim-light (scotopic) photoreceptor rhodopsin belongs to a large group of proteins forming the so-called G protein-coupled receptor (GPCR) family. More specifically, rhodopsin features the common hollow α-helical transmembrane structure of GCPR but hosts an 11-*cis*-retinal chromophore (rPSB11) antagonist covalently connected to the protein via a protonated Schiff base linkage.[1,2] (see Scheme 1).

Scheme 1. Chemical Structure of rPSB11

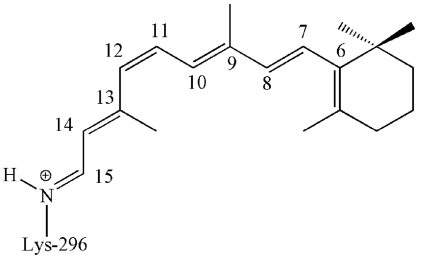

The light-induced (i.e., photochemical) isomerization of the rPSB11 chromophore to its *all-trans* isomer (rPSBAT) is the first step of the so-called rhodopsin photocycle ultimately leading to the production of the protein biologically active Meta-II state.[3]

For a long time, it has been thought that humans cannot perceive infrared (IR) radiation. However, in the 1970s it was discovered that the human retina perceives IR light in the 800−1355 nm range.[4,5] Second harmonic generation[6] in the eye, fluorescence, and two-photon absorption (TPA)[7] were suggested as IR perception mechanisms. Several electrophysiological studies with lower vertebrate photoreceptors revealed nonlinear optical processes leading to rhodopsin activation.[8,9] Although these studies imply that human visual perception might not be limited to the visible part of the electromagnetic spectrum, they did not explain how IR perception is allowed at the molecular level. Thus, their implications for photoreceptor activation, including human photoreceptors, has remained unidentified.

In 2014, Palczewska and co-workers[10] provided evidence that humans can detect IR light at wavelengths around 950−1000 nm and that this is perceived as visible light. The study indicates that IR irradiation causes the photoisomerization of the rPSB11 chromophore, suggesting that IR laser beams could be used to scan the retina and detect eye problems in their early stages, before they become insurmountable, where the using of visible-wavelength lasers might damage the retina.

The present paper is focused on the possibility of computing, rather than measuring, the TPA spectra of rhodopsins using quantum chemistry. To this aim, a theoretical exploration of the TPA properties of Rh using a quantum

Received: August 6, 2019
Accepted: September 23, 2019
Published: September 23, 2019

DOI: 10.1021/acs.jpclett.9b02291
J. Phys. Chem. Lett. 2019, 10, 6293−6300

Table 1. Computed OPA Spectroscopic Properties of Rh with Different Approaches[a]

	vertical (i.e., Franck−Condon) excitation								
	$\langle\Delta E_{S1-S0}\rangle$		$\langle\Delta E_{S2-S0}\rangle$		$\langle\Delta E_{S3-S0}\rangle$		oscillator strength		
method	kcal/mol (nm)	eV	kcal/mol (nm)	eV	kcal/mol (nm)	eV	$\langle\Delta E_{S1-S0}\rangle$	$\langle\Delta E_{S2-S0}\rangle$	$\langle\Delta E_{S3-S0}\rangle$
XMCQDPT2[b]	60.1 (475)	2.60	84.3 (339)	3.65	88.8 (32)	3.85	0.88	0.20	0.20
XMCQDPT2[c]	60.2 (475)	2.61	84.3 (339)	3.65	88.5 (323)	3.83	0.87	0.20	0.21
XMCQDPT2[d]	60.3 (474)	2.61	84.3 (339)	3.65			0.87	0.18	
XMCQDPT2[e]	63.7 (449)	2.76	86.4 (331)	3.75			0.84	0.26	
CASPT2 (IPEA = 0)[f]	57.5 (497)	2.49	83.6 (342)	3.62			0.60	0.38	
expt	57.4 (498)	2.47	84.0 (340)	3.64					

[a]Transition energies (vertical excitation energies) are given in kcal/mol (nm in parentheses) and eV. [b]Average (10 models) 8-root SA with the cc-pVTZ basis set. [c]8-root SA of the representative model (model-6) with the cc-pVTZ basis set. [d]3-root SA of the representative model (model-6) with the cc-pVTZ basis set. [e]3-root SA of the representative model (model-6) with the 6-31G(d) basis set. [f]3-root SA with the 6-31G(d) basis set calculated with MOLCAS.

mechanics/molecular mechanics (QM/MM) model based on multistate multiconfigurational second-order perturbation (MS-MC-PT2) level of QM theory, is carried out. To do so, we focus on the structurally resolved bovine rhodopsin (Rh)[1] dim-light photoreceptor whose amino acid sequence and wavelength of absorption maximum (λ_{max}) are very close to those of human rhodopsin (93% identity and 498[11,12] vs 496[13,14] nm, respectively).

More specifically

(i) We construct ten isolated QM/MM models of Rh based on the previously reported Automatic Rhodopsin Modeling (ARM) protocol[15,16] (see section S1 in the Supporting Information, for computational details) and the XMCQDPT2 (i.e., extended multiconfiguration quasi-degenerate perturbation theory) implementation of the MS-MC-PT2 theory and use it to determine the λ_{max} and intensity (oscillator strength) of the OPA spectra. To assess the model accuracy, we compare the computed and experimental OPA features of Rh.

(ii) By focusing on two previously investigated molecules, *trans*-stilbene and a related stilbenoid,[17−19] we evaluate the reliability of XMCQDPT2 for the simulation of TPA spectra.

(iii) Finally, by using the constructed QM/MM model we compute the Rh TPA spectra and compare it with the available experimental data. The possible photochemical response of the TPA transition is then qualitatively evaluated using semiclassical trajectories.

OPA Properties of the XMCQDPT2/cc-pVTZ//CASSCF/6-31G(d)/AMBER QM/MM Model of Rh. The absorption spectrum of Rh shows three peaks in the UV−vis region.[20] The two principal peaks are located at 498[11] and 280[20,21] nm (57.4 and 102.1 kcal/mol, respectively). The long-wavelength peak is attributed to the $S_0 \rightarrow S_1$ transition[22] and the short-wavelength intense peak is attributed to aromatic amino acids.[20] However, the latter peak is also present in the spectra of rPSB11 in 1,2-dichloroethane solvent[21] with lower intensity. The band at 498 nm corresponds to the lowest $\pi-\pi^*$ transition of the chromophore. There is a weaker peak at 340[12,20,23,24] nm (84.1 kcal/mol) assigned to the $S_0 \rightarrow S_2$ transition,[22] which is only seen in rPSB11.[20]

In Table 1 we report the calculated average vertical excitation energies $\langle\Delta E_{S1-S0}\rangle$, $\langle\Delta E_{S2-S0}\rangle$, and $\langle\Delta E_{S3-S0}\rangle$ computed using the constructed 8-root state average XMCQDPT2/cc-pVTZ//CASSCF/6-31G(d)/AMBER Rh models (the right side of the "//" indicates the level employed for geometry optimization and the left side that used for the energy and property calculations) and compare them to the experimental values obtained by converting wavelengths into vertical excitation energy values. Such excitations involve the ground state (S_0) and the first three singlet excited states (i.e., S_1, S_2, and S_3).

The results show that the $\langle\Delta E_{S1-S0}\rangle$ value is 60.1 ± 0.5 kcal/mol (λ_{max} = 475 ± 4 nm), which differs from the experimental value by less than 3.0 kcal/mol. After looking at the distribution of the positive charge along the chromophore backbone (see Scheme S1 and Table S2 in the Supporting Information) in S_0 and S_1, we see that the positive charge, initially located on the $-N{=}C_{15}-$ moiety, moves forward toward the β-ionone ring and conclude that S_1 has charge transfer character in agreement with previous studies.[22,25,26] The $\langle\Delta E_{S2-S0}\rangle$ value is 84.3 ± 0.4 (λ_{max} = 339 ± 2 nm) that differs from the experimental data by only 0.2 kcal/mol. A similarly low level of discrepancies is also displayed by the corresponding values of the 10 uncorrelated QM/MM models (see section S1 and Table S3 in the Supporting Information), where the errors are in the range of 2.3−3.6 and 0.0−1.0 kcal/mol, respectively. Notice that for ΔE_{S1-S0} these errors are close to the ca. 3.0 kcal/mol blue-shifted error previously documented for ARM generated QM/MM rhodopsin models.[15] Further assessment of the accuracy of the XMCQDPT2 method, the effect of basis set, and variation in the number of contributing roots in the state averaging have been documented in section S4 of the Supporting Information. It is also worth to mention that a comprehensive investigation on the $S_0 \rightarrow S_3$ transition, and the effect of the protein environment on the $S_0 \rightarrow S_2$ and $S_0 \rightarrow S_3$ transitions have been reported in section S5 of the Supporting Information.

TPA Properties of trans-Stilbene and a D−π−A Stilbenoid. The gas-phase *trans*-stilbene (see Scheme S2A in the Supporting Information) and its acceptor−π−donor (A−π−D) derivative 4-(dimethylamino)-4′-nitrostilbene (hereafter referred to as ACCD. See Scheme S2B in the Supporting Information) chromophores were used as benchmarks to validate the protocol for TPA spectra simulation. We selected ACCD because it features a noncentrosymmetric π-conjugation similar to rPSB11. The TPA cross section is related to the imaginary part of the second hyperpolarizability. Hence, our protocol is based on the sum-over-state (SOS) approach and accordingly, the equations "F1" and "D2" in Fortrie et al.[27] have been used to calculate the TPA line-shape as a function of the frequency ω, i.e., the excitation wavelength. Here, the SOS was approximated using 11 intermediate electronic states (12-

DOI: 10.1021/acs.jpclett.9b02291
J. Phys. Chem. Lett. 2019, 10, 6293−6300

Table 2. Calculated and Experimental OPA and TPA Data for *trans*-Stilbene, ACCD, and Rh[a]

		theoretical results				experimental results			
		$\lambda_{max,OPA}$ (nm)	$\lambda_{max,TPA}$ (nm)	σ_{TPA} GM (**au**[b])	Γ_{mn}(eV)		$\lambda_{max,OPA}$ (nm)	$\lambda_{max,TPA}$ (nm)	σ_{TPA} GM
trans-stilbene	this work	292	480	32 (**2033**)	0.2	ref 17	297	514	12
	ref 17[c]	278	466	27	0.1				
	ref 19[d]	267	469; 425	280; 54	0.25	ref 29	302	486	32
	ref 18[e]	471	397−514	117−129	0.2				
	ref 29[f]	273	432	43	0.2				
ACCD	this work	332	664	141 (**9106**)	0.2	ref 30	452 (335)[h]	909	191
	ref 31[g]	404−481		70−149	0.2−0.4				
						ref 32	451	930	114
	ref 33[g]	451		149					
	ref 34	279	∼550	∼30	0.248				
Rh	this work	475	950	472 (**30373**)	0.2	ref 10	498[i]	950−1050[j]	260[l]
	ref 10		1014	2.1				909[k]	

[a] λ_{OPA} and λ_{TPA} (nm) are, respectively, the lowest one-photon absorption wavelength and the two-photon resonance wavelength. σ_{TPA} (GM; 10^{-50} (cm^4 s)/photon-molecule) is the TPA cross section. For the choice of Γ_{mn} value see p 11 in the Supporting Information. [b] Damping factor, Γ_{mn}, cannot be reported in au for literature data due to the different prefactor used to convert microscopic (in au) to macroscopic (in GM) cross section. [c] Theoretical data from the INDO-MRD-CI method. [d] Theoretical data from the CI-CNDO/S method. [e] Theoretical data from the ATDA formalism. [f] Theoretical data from the EOM-EE-CCSD method. [g] Theoretical data from the TDDFT method. [h] The value in parentheses is measured in the vacuum. [i] The value is extracted from ref 11. [j] The value is extracted from ref 10. [k] The value is extracted from ref 35. [l] The value is extracted from ref 36 for ChR2.

root single point calculation, based on previous computations on conjugated chromophores of similar size,[28] see section S1 in the Supporting Information). In our protocol, two absorbed photons in TPA are degenerate, and therefore, the calculated $\lambda_{max,TPA}$ and σ_{TPA} values for *trans*-stilbene (see Figure S4A for the simulated spectra) can be defined as the values corresponding to the maximum of its TPA spectra as in the previous studies[17−19,29] (see Table 2). All calculated data reveal that while the obtained gas-phase $\lambda_{max,TPA}$ values match the experimental value measured in solution (toluene[17] and chloroform[29]) reasonably well, the σ_{TPA} calculated by different methods displays substantial discrepancies (for more discussion see section S1 of the Supporting Informatin), which possibly arise from inconsistent prediction of the transition dipole moments by different computational methods. In fact, comparing with experimental values, our computed TPA properties ($\lambda_{max,TPA}$ = 480 nm and σ_{TPA} = 32 GM) are in better agreement with the values reported by De Wergifosse et al.,[29] ($\lambda_{max,TPA}$ = 486 nm and σ_{TPA} = 32 GM) rather than with those reported by Brédas et al.,[17] ($\lambda_{max,TPA}$ = 514 nm, and σ_{TPA} = 12 GM). Furthermore, comparing to those computed with other methods,[18,19,29] XMCQDPT2 calculations show the best agreement with the experimental data reported by Wergifosse et al.[29]

The TPA spectra of *trans*-stilbene (see Figure S4A) show a peak centered at the $\lambda_{max,TPA}$ = 480 nm that corresponds to the $S_0 \rightarrow S_4$ transition. According to our calculations, appreciable transition dipole moments from S_0 are found only for $S_0 \rightarrow S_1$ (5.7 D) and $S_0 \rightarrow S_3$ (5.0 D) pointing to the fact that the most intense TPA transition of $S_0 \rightarrow S_4$ could happen via the intermediate states S_1 or S_3 (i.e., $S_0 \rightarrow S_1 \rightarrow S_4$ or $S_0 \rightarrow S_3 \rightarrow S_4$, respectively). Inspection of the computed quantities and comparison with the results of the Brédas et al.[17] corroborate the dominant contribution of the $S_0 \rightarrow S_1 \rightarrow S_4$ transition in TPA spectra with the transition dipole moments of 5.7 D for $S_0 \rightarrow S_1$ and 2.5 D for $S_1 \rightarrow S_4$, analogous to that reported in Brédas et al.[17] (i.e., 7.1 and 3.1 D for $S_0 \rightarrow S_1$ and $S_1 \rightarrow S_4$, respectively). In contrast, TDDFT prediction by Nayyar et. al[18] overestimates the $S_1 \rightarrow S_4$ transition dipole moment by a factor of ∼2.6 (8.2 D). This leads to an overestimation of the σ_{TPA} by a factor of ∼5 (note that their reported σ_{TPA} values are in the order of hundred). In conclusion, our gas-phase *trans*-stilbene study indicates that XMCQDPT2 predicts σ_{TPA} in good agreement with the experimental data due to the reasonable values obtained for the transition energies and transition dipole moments.

To understand the effect of molecular geometry on the TPA properties of *trans*-stilbene, we also calculated the spectra at the non-planar MP2/cc-pVTZ-optimized geometry[28] (Figure S5). The result shows a maximum at 486 nm with the σ_{TPA} of 29 GM and, hence, indicates a small effect of the geometry on the transition energies, dipole moments and, consequently, TPA properties of *trans*-stilbene. The geometry of ACCD was then optimized at the MP2/ccpVTZ level and the gas-phase TPA spectra of ACCD was calculated using the same procedure used for *trans*-stilbene due to the complexity of considering the solvent effects. The corresponding TPA spectra are shown in Figure S4B. One of the distinctive features of such D−π−A molecules is the absence of symmetry rules governing optical absorption properties of centrosymmetric molecules, and therefore, any excited state becomes both one- and two-photon allowed. Furthermore, these D−π−A molecules (also known as push−pull molecules) show, in general, larger TPA cross section with respect to *trans*-stilbene.

The calculated OPA vertical excitation energy ($\lambda_{max,OPA}$ = 332 nm, see Table 2) of ACCD, corresponding to the $S_0 \rightarrow S_1$ transition, is in good agreement with the OPA gas-phase measurements (i.e., in a supersonic jet expansion;[37] see Table 2, value in parentheses). This indicates the reliability of our protocol in predicting the OPA properties of D−π−A chromophores. However, this value is far from that of experimental OPA spectra ($\lambda_{max,OPA}$ = 452 nm) in DMSO solvent[30,32] pointing to a solvatochromic effect whose simulation would require an effort going beyond the scope of the present work. Such an effect is expected to cause substantial variations in structure and properties (such as absorption spectra, hyperpolarizabilities, and TPA cross sections). In fact, DFT-based QM/MM calculations[31,33] have

DOI: 10.1021/acs.jpclett.9b02291
J. Phys. Chem. Lett. 2019, 10, 6293−6300

shown that, in contrast to the case of *trans*-stilbene in a nonpolar solvent, a polar solvent (such as DMSO and water) induces geometric distortions that are important to accurate prediction of the OPA and TPA spectra of ACCD. Thus, in principle, when comparing our calculated results to the experiment, it would be important to consider the effects of the medium.[31,33] However, we noticed that the trends in the experimental $\lambda_{max,TPA}$ and σ_{TPA} values when going from *trans*-stilbene to ACCD (486 nm and 32 GM vs. 909 nm and 191 GM, respectively) are qualitatively reproduced with our XMCQDPT2-based methodology (480 nm and 32 GM vs. 664 nm and 141 GM, respectively). We take this as supportive for the protocol qualitative validity for TPA spectra simulation. It is also worth mentioning that our calculated σ_{TPA} value for ACCD is comparable with the value obtained by QM/MM studies probing the solvatochromic effect (see Table 2).[31,33]

TPA Properties of Rh. The predicted σ_{TPA} and $\lambda_{max,TPA}$ values from 10 uncorrelated XMCQDPT2/cc-pVTZ//CASSCF/6-31G(d)/AMBER models of Rh, have allowed us to simulate the TPA band presented in Figure 1. The simulated spectra

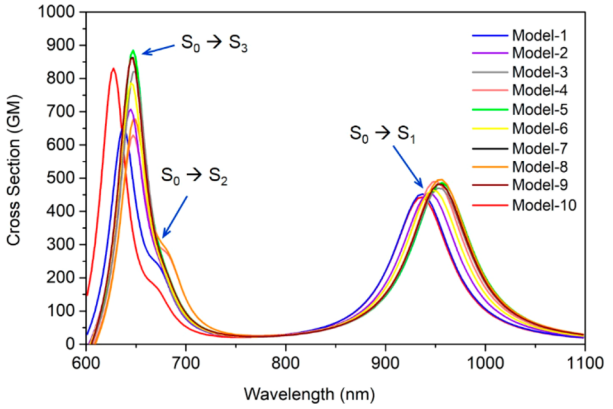

Figure 1. TPA of Rh (rPSB11 embedded in the protein cavity) obtained from 10 QM/MM models at the XMCQDPT2 level of theory (XMCQDPT2/cc-pVTZ//CASSCF/6-31G(d)/AMBER models). The color code matches that in Figure S3.

reflect the blue shift of the OPA spectra of Rh with respect to the gas-phase chromophore[38−40] (Figure S6). The data predict an average TPA cross section of 472 GM at $\lambda_{max,TPA}$ = 950 nm, for the TPA corresponding to the $S_0 \rightarrow S_1$ transition. The calculated σ_{TPA} value is comparable with the relatively high value reported for the close system channelrhodopsin 2 (ChR2), which is ∼260 GM at 920 nm.[36] The predicted $\lambda_{max,TPA}$ value matches the value predicted in a previous theoretical study, reporting an absorption between 950 and 1150 nm with a ∼1000 nm maximum[10] and demonstrating the consistency of such value with experimental electrophysiology data on the sensitivity to IR light of rods and, possibly, cones photoreceptor cells. However, our σ_{TPA} value is different from that computed in the same study. A fact that may be attributed to the use of TDDFT to compute the transition dipole moments or to the choice of macroscopic conversion prefactor. Additionally, analyzing the important orbitals involved in TPA transitions (see section S8 in the Supporting Information for details), consistent with the charge distribution on the rPSB11 chromophore (Table S2 in the Supporting Information), corroborates the charge transfer character of the $S_0 \rightarrow S_1$ transition induced by TPA. Accordingly, as far as incorrect description of the charge-transfer excitations is one of the hallmark failures of TDDFT[41], our protocol is superior for the purpose of reliable prediction of the TPA properties of Rh.

As mentioned above, the computed $\lambda_{max,TPA}$ (∼1000 nm) corresponds to the energy gap of 60.2 kcal/mol results in electronic excitation of the rPSB11 chromophore to its S_1 state. The $S_0 \rightarrow S_1$ vertical excitation corresponds to a $\pi \rightarrow \pi^*$ transition, which is also responsible for the rapid 11-*cis* to *all-trans* photoisomerization of rPSB11.[42] Therefore, in agreement with the results by Palczewska et al.,[10] our calculations corroborate efficient perception of the IR light by Rh and the hypothesis that OPA and TPA result in the same photoisomerization process, producing rPSBAT and therefore activating the Rh photocycle and, in turn, visual perception.[10] This appears to be a straightforward conclusion when considering the computational and experimental evidence in favor of a barrierless nature of the S_1 double-bond isomerization path and the results of semiclassical trajectory simulations as well as time-resolved absorption spectroscopy experiments.[22,43]

OPA and TPA calculations of our Rh QM/MM model demonstrate that while the second excitation ($S_0 \rightarrow S_2$) of the Rh is weak in the OPA spectra (see the oscillator strengths in Table 1), it is somehow more intense in TPA (Figure 1). As is also evident from Table 1, these observations match well with the reported OPA[12,20,23,24] experimental spectra, which show a weak peak at the β band of the Rh corresponding to the $S_0 \rightarrow S_2$ transition. In our study, the calculated average $\lambda_{max,TPA}$ of the Rh models, related to the $S_0 \rightarrow S_2$ transition, is located at 678 ($2 \times \lambda_{max,OPA}$ = 339) nm with the average cross section of 231 GM.

We compared our computed TPA spectra of Rh with the corresponding experimental spectra reported by Birge et al.[35] In that study, the S_1 and S_2 states appear close to each other being ascribed to the ∼490 nm (as appeared in the OPA experiment) and ∼440 nm (appeared in the TPA experiment) values, respectively.[35] On the basis of their experiment, the $\lambda_{max,TPA}$ is 909 nm (11 000 cm^{-1}), which is far from our predictions for the $\lambda_{max,TPA}$ of $S_0 \rightarrow S_2$ but matches well the $\lambda_{max,TPA}$ of $S_0 \rightarrow S_1$. Furthermore, previous experimental studies showed a low-intensity band at 340 nm, which can be assigned to the $S_0 \rightarrow S_2$ transition.[12,20] This assignment is supported by gas-phase[40,44] and our QM/MM calculations, which report well-separated transitions to the S_1 and S_2 states, challenging the S_2 assignment by Birge et al.[35]

The calculated average $\lambda_{max,TPA}$ of our Rh models related to the $S_0 \rightarrow S_3$ transition is located at 644 ($2 \times \lambda_{max,OPA}$ = 322) nm and shows an average σ_{TPA} of 771 GM. Similar to the $S_0 \rightarrow S_2$ transition, the $S_0 \rightarrow S_3$ OPA transition is weak (i.e., it has a small oscillator strength) but, obviously, predicted to be strongly allowed in TPA. Furthermore, while both $S_0 \rightarrow S_2$ and $S_0 \rightarrow S_3$ transitions are predicted to have the same intensity in OPA (i.e., same oscillator strength), the latter has a higher σ_{TPA} (771 GM vs 231 GM). This could be explained in terms of dipole and transition dipole moments used in the sum-over-state (SOS) approach (see section S1, eq 2 in the Supporting Information). After looking at the transition dipole moments (see section S8, Supporting Information), it was found that the most important contributions to the $S_0 \rightarrow S_2$ and $S_0 \rightarrow S_3$ transitions in the TPA spectrum of Rh are $S_0 \rightarrow S_1 \rightarrow S_2$ and $S_0 \rightarrow S_1 \rightarrow S_3$, respectively. The related transition dipole moments are 9.4, 5.0, and 7.5 D for $S_0 \rightarrow S_1$, $S_1 \rightarrow S_2$, and $S_1 \rightarrow S_3$ transitions, respectively. The higher transition dipole moment of $S_1 \rightarrow S_3$ by the factor of ∼1.5 with respect to the S_1

DOI: 10.1021/acs.jpclett.9b02291
J. Phys. Chem. Lett. 2019, 10, 6293−6300

→ S_2 leads to the larger σ_{TPA} of $S_0 \rightarrow S_3$. Looking at the transition diploe moments provides the explanation for different intensity of the $S_0 \rightarrow S_2$ and $S_0 \rightarrow S_3$ transitions in OPA and TPA. In OPA, both the $S_0 \rightarrow S_2$ and $S_0 \rightarrow S_3$ transition dipole moments equal 3.8 D (so the oscillator strengths are quite close too), but in TPA the relevant transition dipole moments differ considerably (9.4, 5.0, and 7.5 D for $S_0 \rightarrow S_1$, $S_1 \rightarrow S_2$, and $S_1 \rightarrow S_3$ transitions, respectively). This also has been justified on the basis of the molecular orbital excitations in section S8 of the Supporting Information.

The dynamics triggered by the population of the S_1, S_2, and S_3 potential energy surfaces has been investigated by computing the corresponding FC trajectories at the CASSCF/6-31G(d)/AMBER level of theory (see section S1 in the Supporting Information, for computational details) which are surface-hop trajectories starting from the S_0 equilibrium structure of our QM/MM representative model (i.e., model-6) with zero initial velocities. The analysis of the geometrical progression along the CASSCF-driven FC trajectories is provided in the Supporting Information (see Figure S8). In order to qualitatively account for the effect of dynamic electron correlation and to be consistent with the above spectral analysis, the energy profiles are also recomputed using the CASPT2//CASSCF/6-31G(d)/AMBER level of theory (Figure 2). As shown in the Figure 2, the shape of the CASPT2 and CASSCF energy profiles for the excited state progression of Rh are similar. However, as expected, the CASPT2 energies are red-shifted due to the inclusion of dynamic electron correlation. FC trajectories provide an approximate description of the motion of the center of the excited state population and, in the present context, are used to provide qualitative evidence that the reactive S_1 state gets populated after TPA to the S_2 and S_3 states.[45] Accordingly, we begin by showing that, with the constructed QM/MM model, the FC trajectory of Rh computed at the two-root state-average CASSCF/6-31G(d)/AMBER level and corrected by three-root state-average CASPT2 level, starting on S_1, reaches the reactive S_1/S_0 conical intersection on a ca. 100 fs time scale (Figure 2A), CI1 and CI1-like points in CASSCF and CASPT2 profiles, respectively) as previously documented with other models for the OPA process.[26,46] This is taken as evidence that the rPSB11 chromophore in the adopted Rh model undergoes isomerization and that the primary photocycle intermediate bathorhodopsin is produced upon decay and relaxation on the S_0 potential energy surface upon IR irradiation. In order to demonstrate that the reactivity is maintained also when populating the S_2 state, we computed the FC trajectory at the same level of theory but employing three-root state-average orbitals in both CASSCF and CASPT2 calculations and starting on S_2 (see Figure 2B). The results indicate that S_1 is populated after ∼15 fs (CI2 and CI2-like in CASSCF and CASPT2 profiles, respectively) upon decay from S_2 to S_1. To provide evidence for a reactive populated region of S_1, we stop the trajectory 10 fs after S_1 population and restart it from the same geometry and velocities and level of theory but with the more accurate two-root state average CASSCF wave function. The S_1 population reaches the reactive S_1/S_0 conical intersection on a ca. 100 fs time scale (Figure 2B, CI1 and CI1-like points in CASSCF and CASPT2 profiles, respectively).

Finally, in order to assess the reactivity of the TPA excitation to S_3 we compute a FC trajectory at the three-root state-average level (from the second to the fourth root) starting

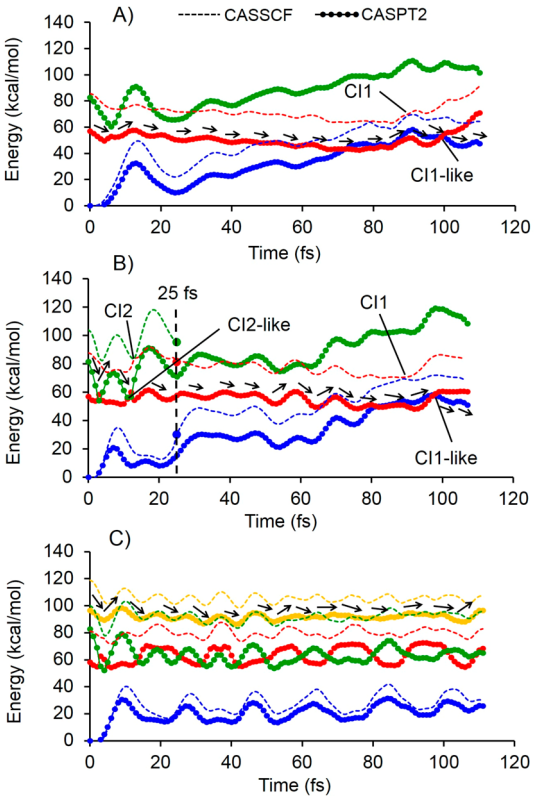

Figure 2. Relative CASSCF (dashed lines) and CASPT2 (solid line + circles) semiclassical energy profiles. (A) Photoisomerization after population of the S_1 state. (B) Photoisomerization after population of the S_2 state. The large full circles and dashed vertical line indicate the change in methodology from three-root to two-root state average in CASSCF energy profiles. (C) Lack of short time scale photoisomerization after population of the S_3 state. CI and CI-like points referred to predicted conical intersection by CASSCF and CASPT2 level of theory, respectively. The stream of black arrows shows the reactive path at each trajectory.

from S_3. We show that the S_3 does not decay after ∼110 fs (see Figure 2C). Accordingly, in contrast with TPA excitation to S_2 and S_1, we see that excitation to S_3 does not yield a fast decay to the S_1 state and hence, a fast S_1-like reactivity (the lack of progress along the isomerization coordinate is documented in the Supporting Information, Figure S8C). A much longer dynamics would be required to establish if this state is bounded (i.e., emissive) or if simply reacts on a much longer time scale.

To summarize, we have simulated the TPA spectra of the dim-light visual receptor Rh, using a set of QM/MM models constructed via a semiautomatic protocol. Such models allow us to use MS-MC-PT2 theory to consistently calculate OPA and TPA spectral properties, ultimately leading to an effective XMCQDPT2/cc-pVTZ//CASSCF/6-31G(d)/AMBER protocol, then validated by comparing computed and experimental quantities for *trans*-stilbene in its C_2 noncentrosymmetric equilibrium geometry and its polar D−π−A derivative ACCD. The comparison shows that the protocol yields transition dipole moments and transition energies and, hence, σ_{TPA} values comparable with experimental data.

The calculated energies and transition dipole moments of the 10 Rh models allowed us to predict an average σ_{TPA} of 472 GM at $\lambda_{max,TPA}$ = 950 nm, for the $S_0 \rightarrow S_1$ transition. This fully supports the hypothesis that a cattle eye and, most likely, the

DOI: 10.1021/acs.jpclett.9b02291
J. Phys. Chem. Lett. 2019, 10, 6293−6300

human eye can detect IR light, which is then perceived as visible light. However, the computed σ_{TPA} value appears to be different from that reported in Palczewska et al.,[10] a fact that may be attributed to the use of TDDFT to calculate the transition dipole moments or to the choice of the macroscopic conversion prefactor.

While the $S_0 \rightarrow S_2$ OPA transition of Rh is very weak, its intensity is increased in the TPA spectrum. More specifically, the computed average σ_{TPA} is 231 GM at $\lambda_{max,TPA}$ = 678 nm. Such a $S_0 \rightarrow S_2$ $\lambda_{max,TPA}$ value appears quite different from the experimentally derived value reported by Birge et al. possibly due to the wrong assignment of the S_2 state as shown in this paper and also pointed out by Andersen et al.[40,44] in the study of the gas-phase rPSB chromophore. However, while a possible contribution to the assignment of the intermolecular charge transfer states (e.g., between the retinal chromophore and a conjugated cavity side chain) cannot be excluded, our QM/MM model is unable to deal with such an event, which will have to be investigated in future work by trying to extend the model QM subsystem.

The capability of two-photon excitation microscopy (TPM) to detect retinal disfunctions has been successfully confirmed in vivo by Palczewska et al.,[47,48] thus showing the potential of two-photon imaging for monitoring early retinoid changes. Due to the possibility of increasing the intrinsic fluorescence of the retinal chromophore via suitable mutations or by using microbial rhodopsins, large cross section values in our calculations assert that rPSB11 could be turned into a fluorescent probe[49] for two-photon microscopy for *in vivo* imaging and monitoring in the red and infrared light regime with the least light-induced damage of living cells. Furthermore, in agreement with the previous experimental studies[50,51] that approve the applicability of near-infrared (NIR) laser (via TPA) to investigate the activation of channelrhodopsin, our model and predicted TPA properties are promising for the computational investigation of rhodopsins (e.g., ChR2) useful in optogenetics.

In conclusion, our calculations show that ca. 950 nm light can be perceived by the green-blue light absorbing Rh photoreceptor at the TPA level, thus supporting the two-photon origin of the IR perception. We also provide evidence, by using semiclassical trajectory calculations, that via TPA Rh can also perceive (see) red light (i.e., close to 678 nm), as the population of S_2 ultimately leads to chromophore isomerization through a conventional S_1 path. However, the TPA population of S_3 may not lead to chromophore isomerization with the same speed as S_2 and S_1 population. Therefore, it is likely that TPA-based perception of a wavelength of 643 nm (ca. orange light) cannot be detected with the same type of mechanism or occur through a significantly slower reaction channel.

■ ASSOCIATED CONTENT

Supporting Information

The Supporting Information is available free of charge on the ACS Publications website at DOI: 10.1021/acs.jpclett.9b02291.

Computational details for methodology, figures of general workflow and general scheme of Rh QM/MM model, tables of excitation energies, charge distribution on the rPSB11 chromophore, further assessment on the accuracy of the QM/MM models, chemical structures, TPA spectra of reference molecules, OPA and TPA properties of rPSB11 in vacuum, transition dipole moments, principal configurations, molecular orbitals, BLA, dihedrals and HOOP profiles along the FC trajectories (PDF)

■ AUTHOR INFORMATION

Corresponding Authors

*E-mail: ioffe@thermo.chem.msu.ru.

*E-mail: molivuc@bgsu.edu.

ORCID

Samira Gholami: 0000-0002-8133-0890

Laura Pedraza-González: 0000-0002-9806-236X

Massimo Olivucci: 0000-0002-8247-209X

Author Contributions

The manuscript was written through contributions of all authors. All authors have given approval to the final version of the manuscript.

Funding

NIH (National Institute of Health) grant number NIH GM126627 01 NSF (National Science Foundation) grant number NSF CHE-CLP-1710191

Notes

The authors declare no competing financial interest.

■ ACKNOWLEDGMENTS

We are grateful to Krzysztof Palczewski for hepful discussion. The research has been supported by the following grants NSF CHE-CLP-1710191 and NIH GM126627 01. M.O. is grateful for a USIAS 2015 grant. S.G., X.Y., and M.O. thank the Ohio Suprcomputer Center for awarded computational resources. M.O. and L.P.-G. are also grateful for a Department of Excellence Grant 2018-2022 from the italian MIUR. The research was carried out partly using the equipment of the shared research facilities of HPC computing resources at Lomonosov Moscow State University.

■ ABBREVIATIONS

TPA, two-photon absorption; OPA, one-photon absorption; Rh, bovine rhodopsin; XMCQDPT2, extended multiconfiguration quasi-degenerate second-order perturbation theory; QM/MM, quantum mechanic/molecular mechanic; rPSB11, 11-*cis*-retinal chromophore; ChR2, channelrhodopsin-2; DFT, density functional theory; TDDFT, time dependent density functional theory

■ REFERENCES

(1) Okada, T.; Sugihara, M.; Bondar, A.-N.; Elstner, M.; Entel, P.; Buss, V. The retinal conformation and its environment in rhodopsin in light of a new 2.2 Å crystal structure. *J. Mol. Biol.* **2004**, *342* (2), 571−583.

(2) Wald, G. The molecular basis of visual excitation. *Nature* **1968**, *219* (5156), 800.

(3) Palings, I.; Pardoen, J. A.; Van den Berg, E.; Winkel, C.; Lugtenburg, J.; Mathies, R. A. Assignment of fingerprint vibrations in the resonance Raman spectra of rhodopsin, isorhodopsin, and bathorhodopsin: implications for chromophore structure and environment. *Biochemistry* **1987**, *26* (9), 2544−2556.

(4) Dmitriev, V. G.; Emel'yanov, V.; Kashintsev, M.; Kulikov, V. V.; Solov'ev, A.; Stel'makh, M.; Cherednichenko, O. B. Nonlinear perception of infrared radiation in the 800−1355 nm range with human eye. *Sov. J. Quantum Electron.* **1979**, *9* (4), 475.

DOI: 10.1021/acs.jpclett.9b02291
J. Phys. Chem. Lett. 2019, 10, 6293−6300

(5) Sliney, D. H.; Wangemann, R. T.; Franks, J. K.; Wolbarsht, M. L. Visual sensitivity of the eye to infrared laser radiation. *J. Opt. Soc. Am.* **1976**, *66* (4), 339−341.
(6) Zaidi, Q.; Pokorny, J. Appearance of pulsed infrared light: second harmonic generation in the eye. *Appl. Opt.* **1988**, *27* (6), 1064−1068.
(7) Denk, W.; Strickler, J. H.; Webb, W. W. Two-photon laser scanning fluorescence microscopy. *Science* **1990**, *248* (4951), 73−76.
(8) Gray-Keller, M.; Denk, W.; Shraiman, B.; Detwiler, P. B. Longitudinal spread of second messenger signals in isolated rod outer segments of lizards. *J. Physiol.* **1999**, *519* (3), 679−692.
(9) Euler, T.; Hausselt, S. E.; Margolis, D. J.; Breuninger, T.; Castell, X.; Detwiler, P. B.; Denk, W. Eyecup scope—optical recordings of light stimulus-evoked fluorescence signals in the retina. *Pfluegers Arch.* **2009**, *457* (6), 1393−1414.
(10) Palczewska, G.; Vinberg, F.; Stremplewski, P.; Bircher, M. P.; Salom, D.; Komar, K.; Zhang, J.; Cascella, M.; Wojtkowski, M.; Kefalov, V. J. Human infrared vision is triggered by two-photon chromophore isomerization. *Proc. Natl. Acad. Sci. U. S. A.* **2014**, *111* (50), E5445−E5454.
(11) Morrow, J. M.; Castiglione, G. M.; Dungan, S. Z.; Tang, P. L.; Bhattacharyya, N.; Hauser, F. E.; Chang, B. S. An experimental comparison of human and bovine rhodopsin provides insight into the molecular basis of retinal disease. *FEBS Lett.* **2017**, *591* (12), 1720−1731.
(12) Crouch, R.; Purvin, V.; Nakanishi, K.; Ebrey, T. Isorhodopsin II: artificial photosensitive pigment formed from 9, 13-dicis retinal. *Proc. Natl. Acad. Sci. U. S. A.* **1975**, *72* (4), 1538−1542.
(13) Katai, N.; Kikuchi, T.; Shibuki, H.; Kuroiwa, S.; Arai, J.; Kurokawa, T.; Yoshimura, N. Caspaselike proteases activated in apoptotic photoreceptors of Royal College of Surgeons rats. *Investig. Ophthalmol. Vis. Sci.* **1999**, *40* (8), 1802−1886.
(14) van Kuijk, F.; Lewis, J.; Buck, P.; Parker, K.; Kliger, D. Spectrophotometric quantitation of rhodopsin in the human retina. *Investig. Ophthalmol. Vis. Sci.* **1991**, *32* (7), 1962−1967.
(15) Melaccio, F.; del Carmen Marín, M.; Valentini, A.; Montisci, F.; Rinaldi, S.; Cherubini, M.; Yang, X.; Kato, Y.; Stenrup, M.; Orozco-Gonzalez, Y. Toward automatic rhodopsin modeling as a tool for high-throughput computational photobiology. *J. Chem. Theory Comput.* **2016**, *12* (12), 6020−6034.
(16) Pedraza-González, L.; De Vico, L.; Marín, M. a. d. C.; Fanelli, F.; Olivucci, M. a-ARM: Automatic Rhodopsin Modeling with Chromophore Cavity Generation, Ionization State Selection, and External Counterion Placement. *J. Chem. Theory Comput.* **2019**, *15* (5), 3134−3152.
(17) Albota, M.; Beljonne, D.; Brédas, J.-L.; Ehrlich, J. E.; Fu, J.-Y.; Heikal, A. A.; Hess, S. E.; Kogej, T.; Levin, M. D.; Marder, S. R. Design of organic molecules with large two-photon absorption cross sections. *Science* **1998**, *281* (5383), 1653−1656.
(18) Nayyar, I. H.; Masunov, A. m. E.; Tretiak, S. Comparison of TD-DFT methods for the calculation of two-photon absorption spectra of oligophenylvinylenes. *J. Phys. Chem. C* **2013**, *117* (35), 18170−18189.
(19) Morel, Y.; Irimia, A.; Najechalski, P.; Kervella, Y.; Stephan, O.; Baldeck, P. L.; Andraud, C. Two-photon absorption and optical power limiting of bifluorene molecule. *J. Chem. Phys.* **2001**, *114* (12), 5391−5396.
(20) Ebrey, T. G.; Honig, B. Ultraviolet chromophore transitions in the rhodopsin spectrum. *Proc. Natl. Acad. Sci. U. S. A.* **1972**, *69* (7), 1897−1899.
(21) Erickson, J. O.; Blatz, P. E. N-retinylidene-1-amino-2-propanol: a Schiff base analog for rhodopsin. *Vision Res.* **1968**, *8* (10), 1367−1375.
(22) Frutos, L. M.; Andruniów, T.; Santoro, F.; Ferré, N.; Olivucci, M. Tracking the excited-state time evolution of the visual pigment with multiconfigurational quantum chemistry. *Proc. Natl. Acad. Sci. U. S. A.* **2007**, *104* (19), 7764−7769.
(23) Shichi, H. Biochemistry of visual pigments II. Phospholipid requirement and opsin conformation for regeneration of bovine rhodopsin. *J. Biol. Chem.* **1971**, *246* (20), 6178−6182.
(24) Rafferty, C. N.; Cassim, J. Y.; McConnell, D. G. Circular dichroism, optical rotatory dispersion, and absorption studies on the conformation of bovine rhodopsin in situ and solubilized with detergent. *Biophys. Struct. Mech.* **1977**, *2* (4), 277−320.
(25) Cembran, A.; Bernardi, F.; Olivucci, M.; Garavelli, M. The retinal chromophore/chloride ion pair: Structure of the photoisomerization path and interplay of charge transfer and covalent states. *Proc. Natl. Acad. Sci. U. S. A.* **2005**, *102* (18), 6255−6260.
(26) Manathunga, M.; Yang, X.; Orozco-Gonzalez, Y.; Olivucci, M. Impact of Electronic State Mixing on the Photoisomerization Time Scale of the Retinal Chromophore. *J. Phys. Chem. Lett.* **2017**, *8* (20), 5222−5227.
(27) Fortrie, R.; Chermette, H. Two-photon absorption strength: A new tool for the quantification of two-photon absorption. *J. Chem. Phys.* **2006**, *124* (20), 204104.
(28) Ioffe, I.; Granovsky, A. Photoisomerization of stilbene: The detailed XMCQDPT2 treatment. *J. Chem. Theory Comput.* **2013**, *9* (11), 4973−4990.
(29) De Wergifosse, M.; Houk, A. L.; Krylov, A. I.; Elles, C. G. Two-photon absorption spectroscopy of trans-stilbene, cis-stilbene, and phenanthrene: Theory and experiment. *J. Chem. Phys.* **2017**, *146* (14), 144305.
(30) Antonov, L.; Kamada, K.; Ohta, K.; Kamounah, F. S. A systematic femtosecond study on the two-photon absorbing D-π-A molecules−π-bridge nitrogen insertion and strength of the donor and acceptor groups. *Phys. Chem. Chem. Phys.* **2003**, *5* (6), 1193−1197.
(31) Arul Murugan, N.; Kongsted, J.; Rinkevicius, Z.; Aidas, K.; Mikkelsen, K. V.; Agren, H. Hybrid density functional theory/molecular mechanics calculations of two-photon absorption of dimethylamino nitro stilbene in solution. *Phys. Chem. Chem. Phys.* **2011**, *13* (27), 12506−12516.
(32) Wielgus, M.; Bartkowiak, W.; Samoc, M. Two-photon solvatochromism. I. Solvent effects on two-photon absorption cross section of 4-dimethylamino-4′-nitrostilbene (DANS). *Chem. Phys. Lett.* **2012**, *554*, 113−116.
(33) Lu, S.-I. Discrete Solvent Reaction Field Calculations for One- and Two-Photon Absorptions of Solution-Phase Dimethylamino Nitro Stilbene Molecule. *J. Phys. Chem. A* **2019**, *123*, 5334.
(34) Ohta, K.; Antonov, L.; Yamada, S.; Kamada, K. Theoretical study of the two-photon absorption properties of several asymmetrically substituted stilbenoid molecules. *J. Chem. Phys.* **2007**, *127* (8), 084504.
(35) Birge, R. R.; Murray, L. P.; Pierce, B. M.; Akita, H.; Balogh-Nair, V.; Findsen, L. A.; Nakanishi, K. Two-photon spectroscopy of locked-11-cis-rhodopsin: evidence for a protonated Schiff base in a neutral protein binding site. *Proc. Natl. Acad. Sci. U. S. A.* **1985**, *82* (12), 4117−4121.
(36) Rickgauer, J. P.; Tank, D. W. Two-photon excitation of channelrhodopsin-2 at saturation. *Proc. Natl. Acad. Sci. U. S. A.* **2009**, *106*, 15025.
(37) Rijkenberg, R.; Bebelaar, D.; Buma, W.; Hofstraat, J. Isolated building blocks of photonic materials: High-resolution spectroscopy of excited states of jet-cooled push-pull stilbenes. *J. Phys. Chem. A* **2002**, *106* (11), 2446−2456.
(38) Sekharan, S.; Weingart, O.; Buss, V. Ground and excited states of retinal Schiff base chromophores by multiconfigurational perturbation theory. *Biophys. J.* **2006**, *91* (1), L07−L09.
(39) Andersen, L. H.; Nielsen, I. B.; Kristensen, M. B.; El Ghazaly, M. O.; Haacke, S.; Nielsen, M. B.; Petersen, M. Å. Absorption of Schiff-base retinal chromophores in vacuo. *J. Am. Chem. Soc.* **2005**, *127* (35), 12347−12350.
(40) Knudsen, J. L.; Kluge, A.; Bochenkova, A. V.; Kiefer, H. V.; Andersen, L. H. The UV-visible action-absorption spectrum of all-trans and 11-cis protonated Schiff base retinal in the gas phase. *Phys. Chem. Chem. Phys.* **2018**, *20* (10), 7190−7194.

DOI: 10.1021/acs.jpclett.9b02291
J. Phys. Chem. Lett. 2019, 10, 6293−6300

(41) Kümmel, S. Charge-Transfer Excitations: A Challenge for Time-Dependent Density Functional Theory That Has Been Met. *Adv. Energy Mater.* **2017**, *7* (16), 1700440.
(42) González-Luque, R.; Garavelli, M.; Bernardi, F.; Merchán, M.; Robb, M. A.; Olivucci, M. Computational evidence in favor of a two-state, two-mode model of the retinal chromophore photoisomerization. *Proc. Natl. Acad. Sci. U. S. A.* **2000**, *97* (17), 9379−9384.
(43) Schapiro, I.; Ryazantsev, M. N.; Frutos, L. M.; Ferré, N.; Lindh, R.; Olivucci, M. The ultrafast photoisomerizations of rhodopsin and bathorhodopsin are modulated by bond length alternation and HOOP driven electronic effects. *J. Am. Chem. Soc.* **2011**, *133* (10), 3354−3364.
(44) Nielsen, I. B.; Lammich, L.; Andersen, L. H. S 1 and S 2 excited states of gas-phase Schiff-base retinal chromophores. *Phys. Rev. Lett.* **2006**, *96* (1), 018304.
(45) Gozem, S.; Luk, H. L.; Schapiro, I.; Olivucci, M. Theory and Simulation of the Ultrafast Double-Bond Isomerization of Biological Chromophores. *Chem. Rev.* **2017**, *117*, 13502−13565.
(46) Luk, H. L.; Melaccio, F.; Rinaldi, S.; Gozem, S.; Olivucci, M. Molecular bases for the selection of the chromophore of animal rhodopsins. *Proc. Natl. Acad. Sci. U. S. A.* **2015**, *112* (50), 15297−15302.
(47) Palczewska, G.; Golczak, M.; Williams, D. R.; Hunter, J. J.; Palczewski, K. Endogenous fluorophores enable two-photon imaging of the primate eye. *Invest. Ophthalmol. Visual Sci.* **2014**, *55* (7), 4438−4447.
(48) Palczewska, G.; Dong, Z.; Golczak, M.; Hunter, J. J.; Williams, D. R.; Alexander, N. S.; Palczewski, K. Noninvasive two-photon microscopy imaging of mouse retina and retinal pigment epithelium through the pupil of the eye. *Nat. Med.* **2014**, *20* (7), 785.
(49) Marín, M. a. d. C.; Agathangelou, D.; Orozco-Gonzalez, Y.; Valentini, A.; Kato, Y.; Abe-Yoshizumi, R.; Kandori, H.; Choi, A.; Jung, K.-H.; Haacke, S. Fluorescence enhancement of a microbial rhodopsin via electronic reprogramming. *J. Am. Chem. Soc.* **2019**, *141* (1), 262−271.
(50) Mohanty, S. K.; Reinscheid, R. K.; Liu, X.; Okamura, N.; Krasieva, T. B.; Berns, M. W. In-depth activation of channelrhodopsin 2-sensitized excitable cells with high spatial resolution using two-photon excitation with a near-infrared laser microbeam. *Biophys. J.* **2008**, *95* (8), 3916−3926.
(51) Andrasfalvy, B. K.; Zemelman, B. V.; Tang, J.; Vaziri, A. Two-photon single-cell optogenetic control of neuronal activity by sculpted light. *Proc. Natl. Acad. Sci. U. S. A.* **2010**, *107* (26), 11981−11986.

DOI: 10.1021/acs.jpclett.9b02291
J. Phys. Chem. Lett. 2019, 10, 6293−6300